Missing-row surface reconstruction of Au(113) induced by adsorbed calcium atoms

Q. T. Jiang and T. Gustafsson
Department of Physics and Astronomy, Rutgers–The State University of New Jersey, P.O. Box 849, Piscataway, New Jersey 08855-0849
and Laboratory for Surface Modification, Rutgers–The State University of New Jersey, P.O. Box 849, Piscataway, New Jersey 08855-0849

P. Häberle
Departmento de Física, Universidad Técnica Federico Santa María, Casilla 110-V, Valparaíso, Chile

D. M. Zehner
Solid State Division, Oak Ridge National Laboratory, Oak Ridge, Tennessee 37831-6057
(Received 8 January 1992)

We report the structure of the (1×2) reconstruction induced by 0.1 monolayer of Ca atoms on the Au(113) surface, using medium-energy ion scattering. Our data show that the (1×2) surface corresponds to a missing-row-type reconstruction. Monte Carlo simulations of the experiment provide a quantitative measurement of the atomic positions at the surface. All the displacements in the surface region are such that the resulting structure smooths out the corrugation inherent in a missing-row reconstruction. We discuss the relation between this reconstruction and the energy balance between competing surface-electronic-charge densities.

I. INTRODUCTION

It is well established that Au surfaces are easily deformed. Surface diffusion of Au atoms at room temperature has been observed in real time by scanning tunneling microscopy (STM).[1] Au is the only metal for which all three low-index surfaces reconstruct at room temperature: The (100) surface forms a $c(26\times68)$,[2–5] the (111) forms a $(23\times\sqrt{3})$,[6–8] and the (110) surface forms a (1×2) (missing-row) reconstruction.[9–12] In addition, application of external perturbations can induce new arrangements of the surface atoms: the (111) and the (110) surfaces undergo phase transitions at fairly modest temperatures[8,13] and by depositing a very small amount of alkali metal (5% of a monolayer) on the (110) surface, a $(1\times2)\rightarrow(1\times3)$ transition can be induced.[14]

While the three low-index fcc surfaces all have at least two mirror planes, the fcc (113) surface has only one such plane. The reduced symmetry of this surface allows the atoms to possibly rearrange themselves in many ways, and specifically a lateral registry shift is symmetry allowed. The description of the surface structure requires then the determination of many structural parameters. In all the fcc (113) surfaces studied to date [Cu,[15,16] Ni,[17] Al,[18] and Rh (Ref. 19)], the (1×1) bulk symmetry is preserved but the vertical (normal to the surface) atomic displacements are significant (5–15 %). There have been attempts to identify a registry shift in studies of the (113) surfaces of Al,[18] Ni,[17] and Rh,[19] but, within error, no such effect has been observed.

In this paper, we report a structural analysis of Au(113), performed using medium-energy ion scattering (MEIS), a powerful quantitative surface structural analysis technique. Due to the factors alluded to above, the Au(113) surface should provide a perhaps even better opportunity to observe a surface registry shift and/or other interesting structural effects. The presence of small concentrations of Ca at the surface (contained in our sample as a bulk impurity and easily segregated to the surface) stabilizes a (1×2) reconstruction, while the LEED patterns from the *clean* surface that we have obtained so far show evidence for more complex structures. We have determined the structure of this (1×2) reconstruction with special emphasis on the existence of a lateral shift.

The plan of this paper is as follows. The experimental procedure is introduced in Sec. II, while the data are presented in Sec. III. We discuss our results in Sec. IV and state our conclusions in Sec. V.

II. EXPERIMENT

Medium-energy ion scattering (MEIS) with *channeling* and *blocking* is a quantitative technique for surface studies.[20] A strength of the technique is that it is often possible to determine some important surface structural effects merely by inspecting the data. The single crystalline sample is oriented in such a way that the incident ions, usually protons, strike the surface along a crystallographic direction. Under such circumstances, the top-most atoms of the rows parallel to the incidence direction of the ion beam shadow atoms in deeper layer. Due to thermal vibrations and/or surface distortions, some of these deeper layer atoms are partially visible to the ion beam. For a given surface and incidence direction, the probability of hitting an atom in a deeper layer is deter-

mined by two factors: the energy of the incoming ions and the surface Debye temperature. In a channeling configuration, typically, only the first two or three atoms along a row have nonzero hitting probabilities. Therefore the surface sensitivity of MEIS is extremely high.

Backscattered ions from the deeper layers can exit the crystal freely in all directions, except along or close to the crystal axes, where blocking from the top layers results in significant reductions in the backscattered ion yield. Therefore, the angular distribution of MEIS contains straightforward information of the surface structure.

Since the scattering cross section for ions, particularly protons, is well known for the ranges of energies used in MEIS,[21-23] the backscattered ion yield can be expressed in absolute units, most conveniently in terms of the number of atoms per unit cell visible to the incident ion beam at the detector. Detailed structural parameters are obtained through Monte Carlo simulations of the experiment. By varying the structural parameters and comparing the outcome of the simulations with the experimental data through an R-factor analysis,[24] the optimal structure can be found. Details of the procedure we use have been described elsewhere.[25]

Aside from the purely structural parameters, the major unknowns in a MEIS experiment are the vibrational properties of the surface atoms. In our simulations, we take the vibrational correlations between the surface atoms into consideration in a two-body approximation by rescaling the uncorrelated vibrational amplitude U as $U'=U\sqrt{1-C}$, where U' is the relative vibrational amplitude and C is the correlation coefficient between adjacent atoms along the incident direction. Both U and C are calculated within the Debye model.[26-28] We have previously used this approximation in MEIS studies of other metal surfaces.[12,14,25,29,30] In this model, the correlation coefficient C is calculated to be 0.38 for ions incident along $[10\bar{1}]$ and $[0\bar{1}\,\bar{1}]$ in the $(1\bar{1}1)$ plane, and 0.20 and 0.23 for ions incident along $[11\bar{2}]$ and [001], respectively, in the $(1\bar{1}0)$ plane.

The Au(113) crystal was cut and oriented to within $\pm 0.3°$ of the desired direction. After mechanical and electrochemical polishing, the sample was mounted in a UHV chamber with a base pressure of $\sim 2\times 10^{-10}$ Torr, equipped with a high-resolution electrostatic toroidal energy analyzer to collect the backscattered ions (angular acceptance $=24°$, energy and angular resolutions $=0.4\%$ and 0.3°, respectively). The surface was cleaned by sputtering, followed by annealing to 700 or 900 K. The cleanliness of the surface was monitored using Auger electron spectroscopy with a double-pass cylindrical mirror analyzer. After annealing to 900 K for 15 min, we found that a reproducible amount of Ca segregates to the surface from the bulk of the crystal. Similar observations have been made by others.[13] The LEED pattern from this surface shows sharp and bright spots with (1×2) symmetry. Mild sputtering can easily remove the Ca atoms from the surface, implying that the Ca atoms only accumulate in the very top region of the sample. When annealing to 700 K, no impurities were detected on the surface. The LEED pattern obtained after this procedure contained satellite reflections along the $[33\bar{2}]$ direction. Unless otherwise noted, we will focus on the (1×2) Ca-induced structure for the rest of this paper.

III. DATA ANALYSIS

A. Missing-row model

The bulk terminated (BT) Au(113) surface is formed by widely spaced close-packed rows of atoms [see Fig. 1(a)]. It is quite similar to an fcc (110) surface but is slightly more open in the direction perpendicular to the close-packed rows (the $[33\bar{2}]$ direction). The separation between the atomic layers perpendicular to the surface is 1.23 Å, which is rather small compared to the separation between the close-packed rows, 4.78 Å. The symmetry of the surface structure is low, with the second atomic layer not centered with respect to the first. Figure 1(b) shows the two equivalent adjacent $(1\bar{1}0)$ mirror planes of the BT fcc (113) surface. Each plane is formed by close-packed rows of atoms extending into the crystal along the $[\bar{1}\,\bar{1}0]$ direction (25.2° off the surface plane).

For a given scattering geometry, the energy loss of a backscattered proton is a simple function of the mass of the target atom. Figure 2 displays the energy spectrum of the ions backscattered from the Ca covered surface

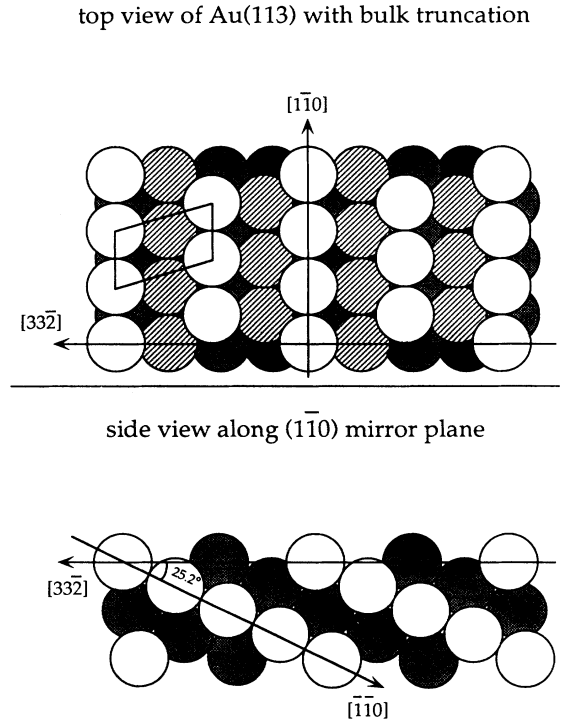

FIG. 1. (a) Top view of the Au(113) surface with bulk truncation. The surface is formed by close-packed rows of atoms along the $[1\bar{1}0]$ direction with a wide separation (4.78 Å) along the $[33\bar{2}]$ direction. Heavier shadings represent deeper layers. The oblique (1×1) unit cell is outlined. (b) The two adjacent $(1\bar{1}0)$ mirror planes. Nearest-neighbor atoms are located along the $[\bar{1}\,\bar{1}0]$ direction, 25.2° off the surface plane, extending into the crystal. The interlayer distance is 1.23 Å. The lattice constant of Au is 4.08 Å.

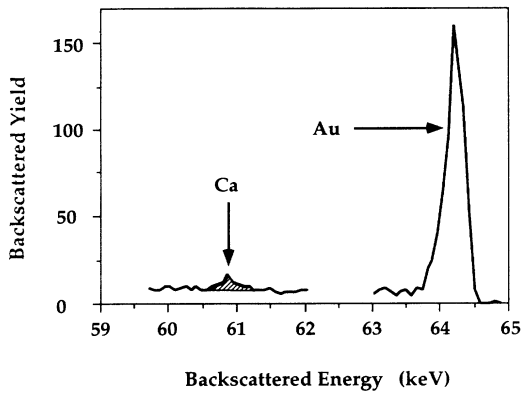

FIG. 2. Energy spectrum of backscattered protons from the Au(113)-(1×2)Ca surface for a 65-keV beam incident along the $[\bar{1}\,\bar{1}0]$ direction. Scattering took place in the $(1\bar{1}0)$ plane, and the backscattered proton flux was collected over 4.5° (30 channels) around the blocking direction corresponding to a 90° scattering angle. The area under the Ca peak is directly proportional to the coverage (0.1 ML).

(annealed to 900 K). Since Au atoms are much heavier than Ca atoms, the protons scattered from Au lose less energy and emerge at the highest energy in the spectrum. The Ca signal, occurring at low energy, is small not only because the amount of Ca is small, but also because the scattering cross section of Ca is smaller than that of Au ($\sigma_{Ca}/\sigma_{Au} \approx \frac{1}{16}$). By evaluating data such as those in Fig. 2, we find that the Ca coverage is (10±5)% of a monolayer [1 ML corresponds to 1 atom/(1×1) unit cell or 7.25×10^{14} atoms/cm^2]. This is an indication that the (1×2) structure must have its origin in a reconstruction of the Au substrate, rather than in an overlayer arrangement.

As mentioned above, the (1×2) Au(110) reconstruction is well understood both theoretically[32–34] and experimentally.[9–12] The basic structure is that of a missing-row (MR) reconstruction with a large inwards relaxation of the top layer atoms and a buckling of the third layer. Figures 3(a) and 3(b) show top and side views of this surface. Although the missing-row structure is more open and corrugated than a bulk truncation, the close-packed microfacets with (111)-type orientations [Fig. 3(b)] make the surface very stable.

Structural models which would appropriately describe the Ca/Au(113) surface should include a (1×2) reconstruction of the Au substate. There is one family of structures based on BT structures (no missing atoms in a layer) which can have a (1×2) symmetry because of a buckling and/or a pairing distortion of the first atomic layer. Even though the separation between the top-layer atomic rows for these particular surfaces is too large to make these kind of correlated distortions physically plausible, we have considered this possibility in the analysis of our data.

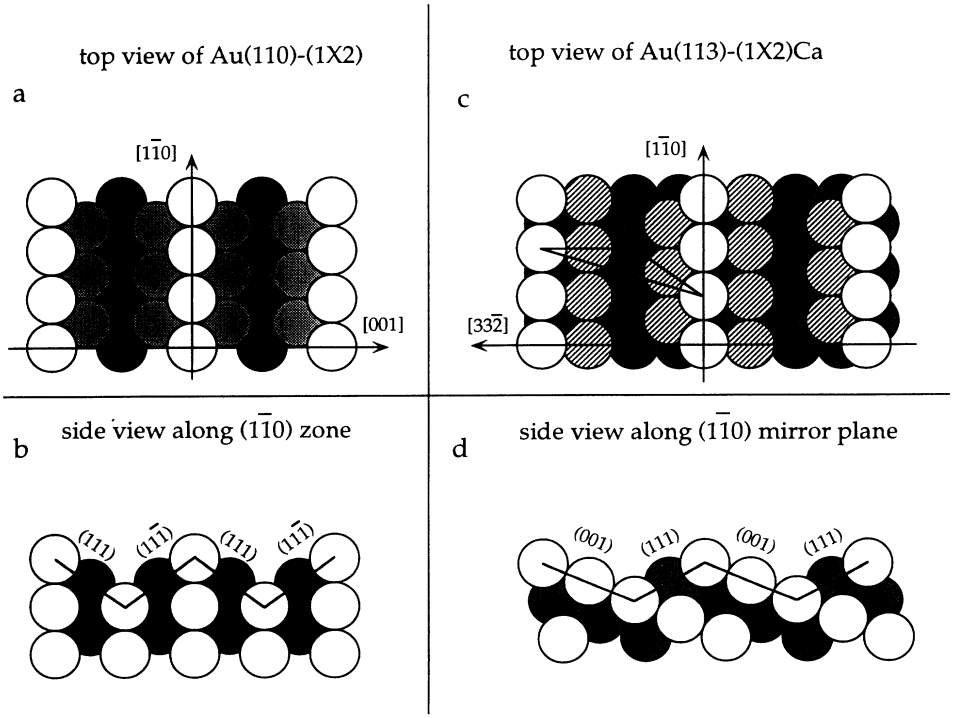

FIG. 3. (a) Top view of the missing-row structure of the Au(110)-(1×2) surface. Every other close-packed row of atoms is missing from the surface. (b) Side view of the Au(110)-(1×2) surface along the $(1\bar{1}0)$ plane. The surface reconstructs to form close-packed microfacets with (111) and $(11\bar{1})$ orientations. (c) Top view of the missing-row structure of the Au(113)-(1×2)Ca surface. The model sensitive scattering plane $(1\bar{1}1)$ is outlined in a triangle. (d) Two adjacent $(1\bar{1}0)$ mirror planes of the missing-row structure of the Au(113)-(1×2)Ca surface. Note that no atoms are missing from one plane (open circles), while all the first-layer atoms are missing from the other plane (solid circles).

By eliminating every other close-packed row of atoms from the BT surface, the missing-row structure for the Au(113) surface is obtained. Figures 3(c) and 3(d) show a schematic representation of this surface structure. The vacancy left in the top layer uncovers the two microfacets which form this structure: the lower (111) and (001) atomic planes.

In order to distinguish between structural models (MR and BT), we need to perform measurements in a scattering plane with the proper sensitivity to the different models. For the MR model shown in Fig. 3(d) all the missing atoms happen to be in one $(1\bar{1}0)$ mirror plane. The data obtained in this scattering plane does not allow one to distinguish between a MR- or a BT-type structure. By using instead a $(1\bar{1}1)$ scattering plane, which has been proven to be a model-sensitive scattering plane on other fcc surfaces,[12,14,29,35] we can obtain a reasonable differentiation between the models. The $(1\bar{1}1)$ scattering plane outlined in the triangle in Fig. 3(c) is not perpendicular to the surface, but tilted 31.4° away from the surface normal.

Figure 4(a) shows the scattering geometry in the $(1\bar{1}1)$ plane. We collected data in this geometry around the [110] direction. The experimental data (open squares) are displayed in Fig. 4(b). It is clear that the blocking dip position is significantly shifted away from the bulk blocking direction (60°) towards smaller angles, implying a large contraction of the first interlayer spacing.

Monte Carlo simulations based on both a relaxed (optimized) missing-row structure and a relaxed (optimized) BT model are displayed in Fig. 4(b). The simulation based on the missing-row structure agrees quite well with our data, while the simulation for the BT overestimates the depth of the blocking dip. This depth is mainly determined by the hitting probability for the second-layer atoms (x) and the blocking efficiency of the top layer atoms on the outgoing path (y). For the BT structure, the depth of the blocking dip (d_{BT}) is approximately given by $d_{BT}=xy$. For the missing-row structure, the hitting probabilities of the two inequivalent second layer atoms in the (1×2) unit cell are 1 and x, and the top layer blocking efficiencies are y and 0 accordingly. Therefore the depth of the blocking dip (d_{MR}) is $d_{MR}=y/2$. Comparing the expressions for d_{BT} and d_{MR}, we find that $x_0=0.5$ is a critical value, and that as long as the surface considered in the simulation allows for a large enough hitting probability of the second-layer atom ($x>x_0$) the

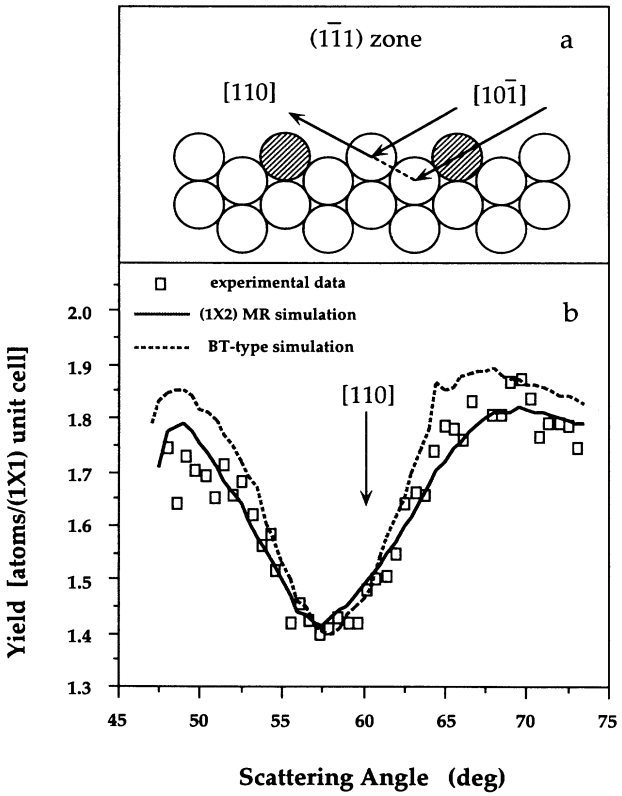

FIG. 4. (a) Scattering geometry for 100-keV protons incident along the $[10\bar{1}]$ direction and detected in an angular range including the [110] direction in the $(1\bar{1}1)$ plane. The shaded atoms are the missing atoms in the missing-row model. (b) The experimental backscattered yield (open squares) and the unsmoothed simulations based on the MR structure (solid line) and the BT structure (dashed line) as a function of scattering angle. The crystallographic direction associated with the bulk blocking dip is indicated.

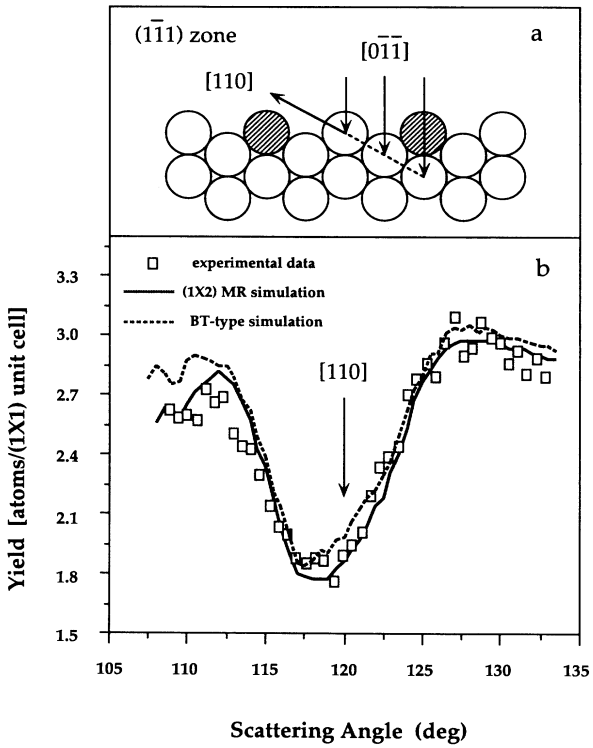

FIG. 5. (a) Scattering geometry for protons incident along the $[0\bar{1}\bar{1}]$ direction and detected in an angular range including the [110] direction in the $(1\bar{1}1)$ plane. The shaded atoms are the missing atoms in the missing-row model. (b) The experimental backscattered yield (open squares) and the unsmoothed simulations based on MR surface (solid line) and BT surface (dashed line) as a function of scattering angle for 100-keV protons. The crystallographic direction associated with the bulk blocking dip is indicated.

depth of the blocking dip for the BT surface is going to be larger than that for the MR structure. If we include the effects from deeper layer atoms, the exact value of x_0 may change.

In our situation, as the $(1\bar{1}1)$ plane is tilted 31.4° away from the normal, the vertical relaxations move the surface atoms away from the scattering plane, leaving deeper layer atoms largely exposed to the incident beam. This implies a high probability of hitting a second layer atom ($x \approx 0.8$ in this case), and as a consequence, simulations based on BT structures overestimate the depth of blocking dip shown by the experimental data.

We also measured the backscattering with ions incident along the $[0\bar{1}\,\bar{1}]$ direction and detected around the [110] direction in the same scattering plane (Fig. 5). We found that the bulk blocking occurs along the [110] direction which corresponds to a scattering angle of 120°. As expected from the surface contraction, the blocking dip is shifted towards smaller angles. Although the incoming ion beam sees deeper into the crystal, thus making the data less surface sensitive, the data still show a better fit for the MR model than for the BT structure.

The ion-scattering measurements in these two scattering geometries clearly favor the missing-row model. In what follows, we will concentrate on the determination of the structural parameters within the MR model for this surface.

B. Structural parameters

In addition to the two scattering geometries considered above, we also performed ion scattering measurements in two other scattering geometries in the $(1\bar{1}0)$ mirror plane. The incident proton beam's directions used in these geometries were $[11\bar{2}]$ and [001]. The backscattered flux for these two different incident angles was collected around the [110] direction. This scattering plane does not distinguish between MR and BT models but is useful in refining the structural parameters within a specific model. We therefore only show optimized Monte Carlo simulation for the MR model with the data in Figs. 6 and 7.

In searching for the global optimum structural parameters, we define the overall R factor value as the root mean square of the four individual R factors for each scattering geometry. The best-fit parameters based on the overall R-factor analysis are close to those extracted from each scattering geometry. The differences between the overall R factor and each individual R factor give us

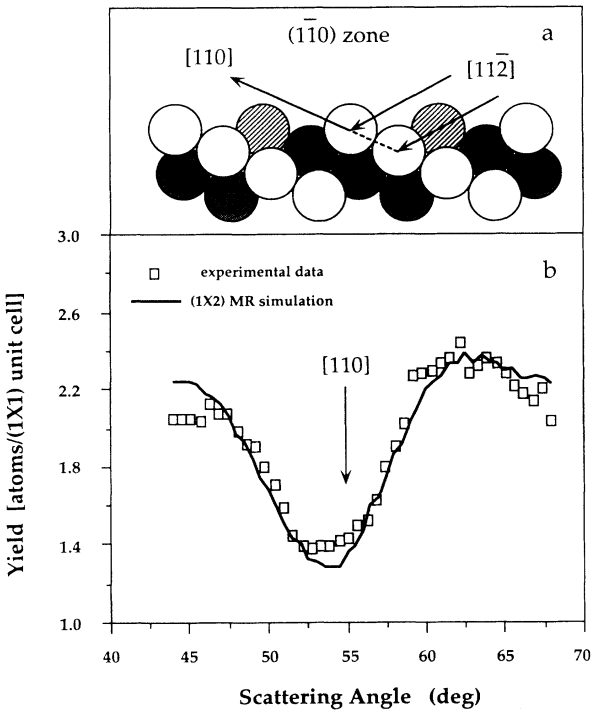

FIG. 6. (a) Scattering geometry for protons incident along the $[11\bar{2}]$ direction and detected in an angular range including the [110] direction in the $(1\bar{1}0)$ plane. The lightly shaded atoms are the missing atoms which are contained in the same plane with the heavily shaded atoms. (b) The experimental data (open squares) and the unsmoothed simulation for our optimum structure (solid line) as a function of scattering angle for 100-keV protons. The crystallographic direction associated with the bulk blocking dip is indicated.

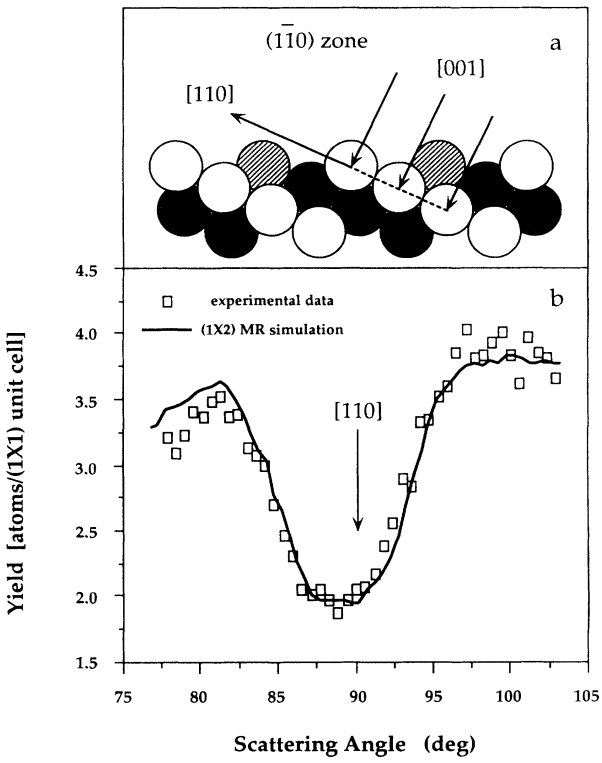

FIG. 7. (a) Scattering geometry for protons incident along the [001] direction and detected in an angular range including the [110] direction in the $(1\bar{1}0)$ plane. The lightly shaded atoms are the missing atoms in the same plane as the heavily shaded atoms. (b) Experimental data (open squares) and the unsmoothed simulation for our optimum structure (solid line) as a function of scattering angle for 100-keV protons. The crystallographic direction associated with the bulk blocking dip is indicated.

the magnitude of the error bars of the measurement.

The contour plots of the (overall) R factor, such as the ones shown in Fig. 8, are examples of the results of searching for optimum parameters. These particular contour plots are obtained using the optimal values for the parameters not varied in these particular plots. In the contour plot shown in Fig. 8(a), the two most sensitive structural parameters (the changes of the top two interlayer spacings, Δd_{12} and Δd_{23}) are varied. A clear minimum exists for $\Delta d_{12}=(-18.6\pm4.5)\%$ and $\Delta d_{23}=(+4.6\pm2.5)\%$. Figure 8(b) shows the contour plot for variations of the second and the third interlayer spacings. The optimum value of the third interlayer spacing is found at the center of the smallest loop with $\Delta d_{34}=(-2.1\pm1.5)\%$. It is encouraging to see that the optimum change in the second interlayer spacing (Δd_{23}) is the same in both plots ($\Delta d_{23}=+4.6\%$), confirming the quality of the fit. The alternate signs of the interlayer distortions are an indication of the oscillatory relaxations commonly found at metal surfaces.

In addition to the relaxations in which atoms stay in crystal planes, atoms can move out of the crystal planes (buckling). A buckling distortion is an alternating displacement of atoms in a particular layer along the direction perpendicular to the surface. Referring to Fig. 3(d), we define the following atomic movements as the positive second- (third-) layer buckling distortion b_2 (b_3): the second- (third-) layer atom in the open circle plane moving upward (along the [113] axis) while the corresponding atom in the filled circle plane moving downward (along the $[\bar{1}\bar{1}\bar{3}]$ axis). The optimum second- and third-layer buckling (b) distortions are found to be, respectively, $b_2=-0.08\pm0.04$ Å and $b_3=+0.08\pm0.04$ Å.

Since the symmetry group of the surface contains only one mirror plane, a surface registry shift along the plane is allowed. We have searched for a registry shift of the first layer and also for a pairing distortion of the second layer. However, in both cases no positive evidence for a surface registry shift or a pairing was obtained. Combined with the small values of registry shifts for other fcc (113) surfaces,[17–19] we are lead to conclude that these surfaces are highly stable towards lateral distortions.

One of the advantages of MEIS is that the data can be put on an absolute basis, with no arbitrary fitting parameters involved. The only nonstructural parameter in the analysis is the surface vibrational amplitude (the bulk vibrational amplitude is 0.090 Å at room temperature). Since half of the bonds are missing for the surface atoms, the surface vibrations are usually found to be enhanced with respect to the bulk vibrations.[20] In this study, we assume the same enhanced vibrational amplitude for the top two layers. Starting form the third layer, we reduce the enhanced part of the vibrational amplitude by a factor of 2 between adjacent layers, and continue this trend into the bulk. The results presented here are not sensitive to the exact way the decay is modeled. By varying the vibrational amplitude in the numerical simulations, the amplitude in the top two layers was found to be enhanced by a factor of 1.55 with respect to the bulk value, which corresponds to a surface Debye temperature of 109 K [the bulk Debye temperature of Au is 170 K (Ref. 36)].

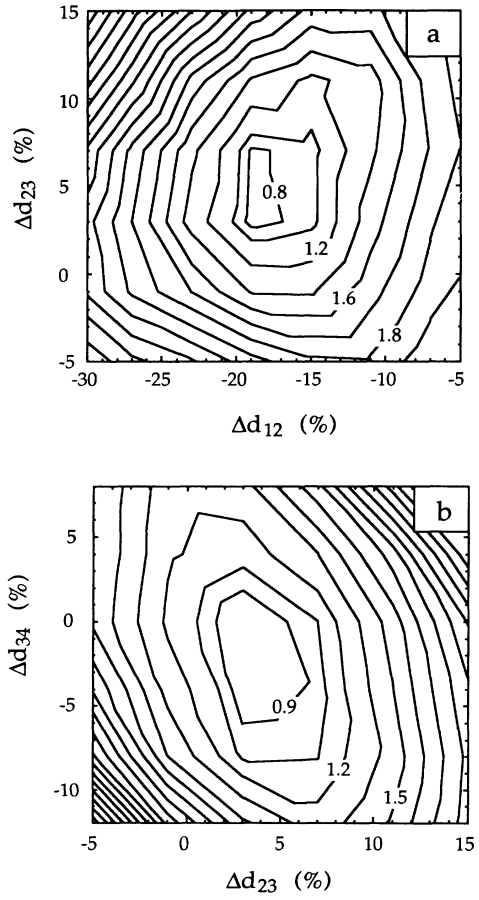

FIG. 8. (a) R-factor contour plot as a function of the changes of the top two interlayer spacings, Δd_{12} and Δd_{23}. (b) R-factor contour plot as a function of the changes of the second and third interlayer spacings Δd_{23} and Δd_{34}. Note that the minimum of the R factor occurs for the same value of Δd_{23} in both plots.

IV. DISCUSSION

A simple comparison of the surface energies of the different atomic planes involved in the MR reconstruction should give an indication of how favorable the MR structure is over bulk termination. As shown in Fig. 3(d), the MR model contains facets with (001) and (111) orientations. The change in the surface energy Δ due to the reconstruction could be estimated by adding the energies of the (001) and (111) atomic planes and subtracting the energy for a BT surface; $\Delta=0.60\gamma(001)+0.52\gamma(111)-\gamma(113)$, where γ denotes the surface energy for a specific orientation. The factors 0.60 and 0.52 come from the increased surface area due to the microfaceting. The stability of the (1×2) missing-row reconstruction requires the energy change Δ to be negative. Theoretical values for $\gamma(001)$ and $\gamma(111)$ are 0.102 eV/Å^2 (Ref. 37) and 0.78 eV/Å^2,[38] respectively. Unfortunately, there is no calculation for $\gamma(113)$ yet. However, $\gamma(110)$ is 0.10 eV/Å^2.[39] If we assume the surface energy of Au(113) is

larger than that of Au(110) due to the fact that the Au(113) surface is more open, e.g., $\gamma(113) > 0.10$ eV/Å^2, the we get $\Delta < 0$. This argument indicates that the formation of (001) and (111) microfacets in the MR Au(113) does lower the surface energy.

The stability of the missing-row reconstruction can be rationalized from a simple argument concerned with the energy balance between the competing surface-electronic-charge densities.[32] For a 5*d* metal such as Au, the surface energy can be heuristically separated into one part coming from the *s* and *p* electrons with delocalized wave functions at the surface, and another part from the localized *d* electrons which includes the bonding (or broken bonds due to missing nearest neighbors) at the surface. The *s* and *p* electrons contribute to the surface kinetic energy and affect largely the relative stability of the different surface structures. As the number of broken *d* bonds remain the same for the (1×1) BT structure and the (1×2) MR structure, the missing-row geometry minimizes the surface energy by providing more room for the *s* and *p* electrons to spread out—thus lowering their kinetic energies, while retaining as much of the bulk cohesion as possible. Upon adding free electron metal atoms like Ca on Au(113) surface, more delocalized electronic charge is introduced onto the surface, thus tilting the energy balance towards a MR reconstruction.

It is expected for metal surfaces that the relaxations alternate sign between layers.[40,41] The values of relaxations found on the Au(113)-(1×2) Ca surface (with $\Delta d_{12} = -18.6\%$, $\Delta d_{23} = +4.6\%$, and $\Delta d_{34} = -2.1\%$) are very close to those found on Au(110).[12] It is also expected that the top-layer contraction of Au(113) (with Ca present) is larger than any of the other studied (113) surfaces: −5.0% for Cu(113),[16] −15.9% for Ni(113),[17] −13% for Al(113),[18] and −14.5% for Rh(113).[19] Previous observations have found that larger distortions are usually present in Au surfaces,[2–4,6–12,14,29,31,34,42] and the more open (1×2) MR surface should show larger distortions than (1×1) surfaces.

Figure 9 shows the major displacements of the surface atoms. In addition to the relaxations, buckling distortions are also present. As a consequence of the buckling ($b_3 = 0.078$ Å), the third-layer atoms move upwards towards the vacancy in the top layer, reducing slightly the surface corrugation. The top-layer contraction and the direction of third-layer buckling in the contiguous atomic plane seem to be related since both occur in the same downwards direction. However, for the second-layer buckling there is no clear structural reason why it should happen, apart from this being a symmetry allowed distortion.

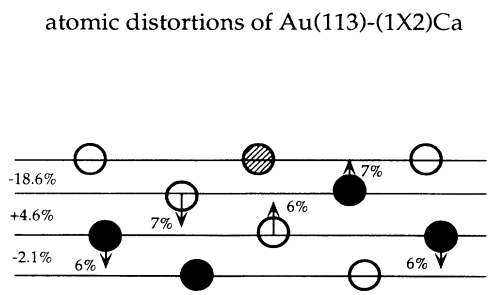

FIG. 9. The surface atomic displacements for the Au(113)-(1×2)Ca surface. The lightly shaded atom is the missing atom in the same plane as the "filled" atoms. The horizontal lines represent the center of the relaxed surface planes, while the arrows represent the buckling distortions on top of the relaxation. The sizes of the arrows are not proportional to the magnitudes of the real displacements.

Based upon the above structural configuration, we calculate the area occupied by each atom in the (111) and (100) microfacets to be $0.835a^2$ and $0.980a^2$ (a is the nearest-neighbor separation for an Au crystal), respectively, while the bulk values are $0.866a^2$ and $1.000a^2$, implying that the two microfacets contract. Comparing the area per atom for the (111) and (100) microfacets to the values for the infinite reconstructed (111) and (100) surfaces ($0.826a^2$ and $0.793a^2$),[8] the values for the (111) microfacet and for the (111) surface are close, while the values for the (100) microfacet and for the (100) surface are quite different. This may indicate that edge effects are important on the (100) microfacet.

One can observe from Fig. 9 that the second- and third-layer bucklings give rise to an interesting pattern of distortions. For any pair of nearest-neighbor atoms in the second and third layer along the $[\bar{1}\,\bar{1}0]$ direction, the change in the interatomic spacing along this direction between nearest-neighbor *pairs* alternates signs. In a simple model, the contraction (expansion) of the interatomic distances along this axis can be related to an excess (deficiency) of charge density between the paired atoms. In this picture the resulting charge density located in the second and third atomic interlayer has a dipolar character which alternates its sign between the [110] rows of atoms. It would be premature to claim that this surface shows a dipolar surface charge density wave based only on the interatomic relaxations pattern, but it would be worth looking for further evidence for such behavior.

Finally, we would like to address the role of Ca on the surface. Due to the small scattering cross section of Ca, it is difficult to determine the exact locations of the Ca atoms at the surface. However, we believe that they stay on top of the surface since the incident ion beam detects roughly the same amount of Ca for different incident directions. The extra low-energy electron diffraction (LEED) spots observed on the clean Au(113) surface may be an indication that the bulk truncated structure is unstable and has a tendency to form higher-order structures.

V. CONCLUSIONS

Using medium-energy ion scattering, we have studied the Ca-induced (1×2) missing-row structure of Au(113). The amount of Ca, segregated from the bulk at 900 K, has been measured with MEIS to be 10% of a monolayer.

The surface exhibits an oscillatory relaxation with a top-layer contraction of $\Delta d_{12} = -18.6\%$, a second-layer expansion of $\Delta d_{23} = +4.6\%$, and a third-layer contraction of $\Delta d_{34} = -2.1\%$. Buckling, with amplitudes of -0.08 and $+0.08$ Å, exist in the second and third layers. Within the error bars of the study, no lateral movement (registry shift or pairing) has been found. All the vertical atomic displacements are such that they smooth the surface corrugation.

ACKNOWLEDGMENTS

We would like to thank Dr. S. Mochrie for lending us the Au(113) crystal, and P. Statiris for his help during the experiment. The work was jointly supported by NSF Grant No. DMR-9019868; FONDECYT Grant No. 0480-90, UTFSM Grant No. 901101, Chile; and Division of Materials Sciences, U.S. DOE Grant No. DE-AC05-84OR21400 with M.M.E.S., Inc.

[1]R. C. Jaklevic and L. Elie, Phys. Rev. Lett. **60**, 120 (1988).
[2]M. A. van Hove, R. J. Koestner, P. C. Stair, J. P. Biberian, L. L. Kesmodel, I. Bartos, and G. A. Somorjai, Surf. Sci. **103**, 189 (1981).
[3]K. H. Rieder, T. Engel, R. H. Swendsen, and M. Manninen, Surf. Sci. **127**, 223 (1983).
[4]G. K. Binnig, H. Rohrer, Ch. Gerber, and E. Stoll, Surf. Sci. **144**, 321 (1984).
[5]X. Gao, A. Hamelin, and M. J. Weaver, Phys. Rev. Lett. **67**, 618 (1991).
[6]M. M. Dovek, C. A. Lang, J. Nogami, and C. F. Quate, Phys. Rev. B **40**, 11 973 (1989).
[7]C. Wöll, S. Chiang, R. J. Wilson, and P. H. Lippel, Phys. Rev. B **39**, 7988 (1989).
[8]A. R. Sandy, S. G. J. Mochrie, D. M. Zehner, K. G. Huang, and Doon Gibbs, Phys. Rev. B **43**, 4667 (1991).
[9]G. Binnig, H. Rohrer, Ch. Gerber, and E. Weibel, Surf. Sci. **131**, L379 (1983).
[10]W. Moritz and D. Wolf, Surf. Sci. **163**, L655 (1985).
[11]H. Hemme and W. Heiland, Nucl. Instrum. Methods B **9**, 41 (1985).
[12]M. Copel and T. Gustafsson, Phys. Rev. Lett. **57**, 723 (1986).
[13]J. C. Campuzano, M. S. Foster, G. Jennings, R. F. Willis, and W. Unertl, Phys. Rev. Lett. **54**, 2684 (1985).
[14]P. Häberle, P. Fenter, and T. Gustafsson, Phys. Rev. B **40**, 5810 (1989).
[15]W. T. Moore, R. W. Streater, D. C. Frost, and K. A. R. Mitchell, Solid State Commun. **24**, 139 (1977).
[16]R. W. Streater, W. T. Moore, P. R. Watson, D. C. Frost, and K. A. R. Mitchell, Surf. Sci. **72**, 744 (1978).
[17]D. L. Adams, W. T. Moore, and K. A. R. Mitchell, Surf. Sci. **149**, 407 (1985).
[18]J. R. Noonan, H. L. Davis, and W. Herley, Surf. Sci. **152**, 142 (1985).
[19]S. Liepold, N. Elbel, M. Michl, W. Nichtl-Pecher, L. Heinz, and K. Müller, Surf. Sci. **240**, 81 (1990).
[20]J. F. van der Veen, Surf. Sci. Rep. **5**, 203 (1985).
[21]G. Moliére, Z. Naturforsch. **2a**, 133 (1947).
[22]J. P. Biersack and J. F. Ziegler, Nucl. Instrum. Methods **194**, 93 (1982).
[23]D. J. O'Connor and J. P. Biersack, Nucl. Instrum. Methods B **15**, 14 (1986).
[24]I. Stensgaard, R. Feidenhans'l, and J. E. Sørensen, Surf. Sci. **128**, 281 (1983).
[25]Q. T. Jiang, P. Fenter, and T. Gustafsson, Phys. Rev. B **44**, 5773 (1991).
[26]R. J. Glauber, Phys. Rev. **98**, 1692 (1955).
[27]D. P. Jackson, B. M. Powell, and G. Dolling, Phys. Lett. **51A**, 87 (1975).
[28]D. P. Jackson and J. H. Barrett, Comput. Phys. Commun. **13**, 157 (1977).
[29]P. Häberle and T. Gustafsson, Phys. Rev. B **40**, 8218 (1989).
[30]Q. T. Jiang, P. Fenter, and T. Gustafsson, Phys. Rev. B **42**, 9291 (1990).
[31]R. Michaelis and D. M. Kolb, Surf. Sci. **234**, L281 (1990).
[32]K.-M. Ho and K. P. Bohnen, Phys. Rev. Lett. **59**, 1833 (1987).
[33]S. P. Chen and A. F. Voter, Surf. Sci. **244**, L107 (1991).
[34]M. Manninen, J. K. Nørskov, and C. Umrigar, Surf. Sci. **88**, L393 (1982).
[35]J. W. M. Frenken, R. L. Krans, J. F. van der Veen, E. Holub-Krappe, and K. Horn, Phys. Rev. B **59**, 2307 (1987).
[36]Colin J. Smithells, *Metals Reference Book* (Plenum, New York, 1967).
[37]F. Ercolessi, E. Tosatti, and M. Parrinello, Phys. Rev. Lett. **57**, 719 (1986).
[38]R. J. Needs and M. Mansfield, J. Phys. Condens. Matter **1**, 7555 (1989).
[39]L. Z. Mezey and J. Giber, Jpn. J. Appl. Phys. **21**, 1569 (1982).
[40]M. W. Finnis and V. Heine, J. Phys. F **4**, L37 (1974).
[41]Uzi Landman, Ross N. Hill, and Mark Mostoller, Phys. Rev. B **21**, 448 (1980).
[42]M. S. Zei, G. Lehmpful, and D. M. Kolb, Surf. Sci **221**, 23 (1989).

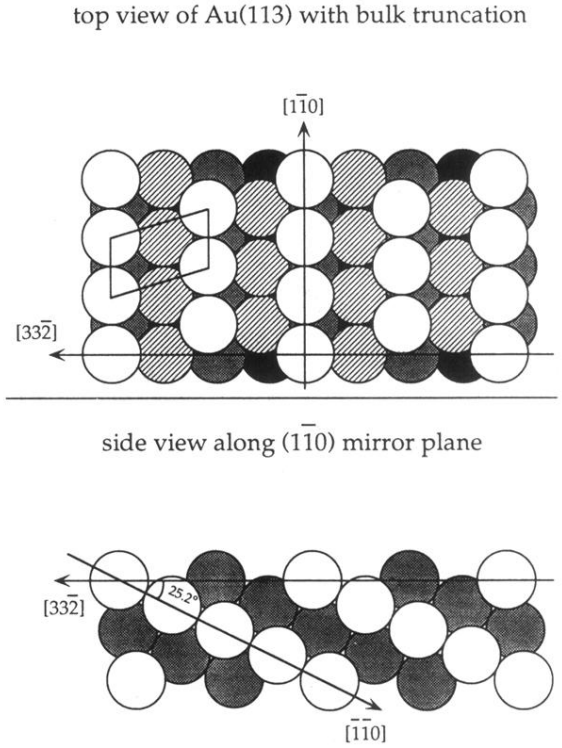

FIG. 1. (a) Top view of the Au(113) surface with bulk truncation. The surface is formed by close-packed rows of atoms along the [1$\bar{1}$0] direction with a wide separation (4.78 Å) along the [33$\bar{2}$] direction. Heavier shadings represent deeper layers. The oblique (1×1) unit cell is outlined. (b) The two adjacent (1$\bar{1}$0) mirror planes. Nearest-neighbor atoms are located along the [$\bar{1}$ $\bar{1}$0] direction, 25.2° off the surface plane, extending into the crystal. The interlayer distance is 1.23 Å. The lattice constant of Au is 4.08 Å.

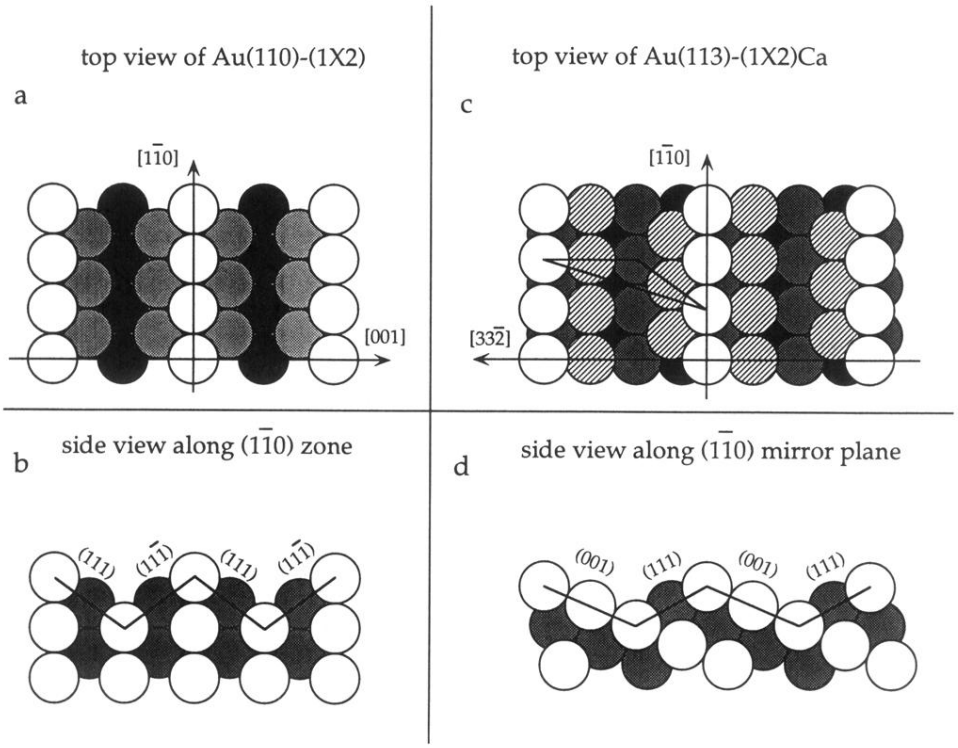

FIG. 3. (a) Top view of the missing-row structure of the Au(110)-(1×2) surface. Every other close-packed row of atoms is missing from the surface. (b) Side view of the Au(110)-(1×2) surface along the (1$\bar{1}$0) plane. The surface reconstructs to form close-packed microfacets with (111) and (11$\bar{1}$) orientations. (c) Top view of the missing-row structure of the Au(113)-(1×2)Ca surface. The model sensitive scattering plane (1$\bar{1}$1) is outlined in a triangle. (d) Two adjacent (1$\bar{1}$0) mirror planes of the missing-row structure of the Au(113)-(1×2)Ca surface. Note that no atoms are missing from one plane (open circles), while all the first-layer atoms are missing from the other plane (solid circles).

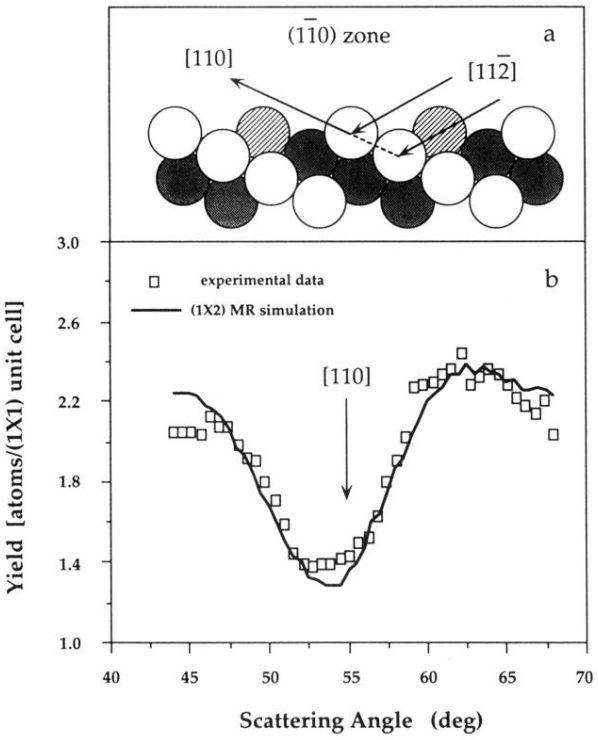

FIG. 6. (a) Scattering geometry for protons incident along the $[11\bar{2}]$ direction and detected in an angular range including the [110] direction in the $(1\bar{1}0)$ plane. The lightly shaded atoms are the missing atoms which are contained in the same plane with the heavily shaded atoms. (b) The experimental data (open squares) and the unsmoothed simulation for our optimum structure (solid line) as a function of scattering angle for 100-keV protons. The crystallographic direction associated with the bulk blocking dip is indicated.

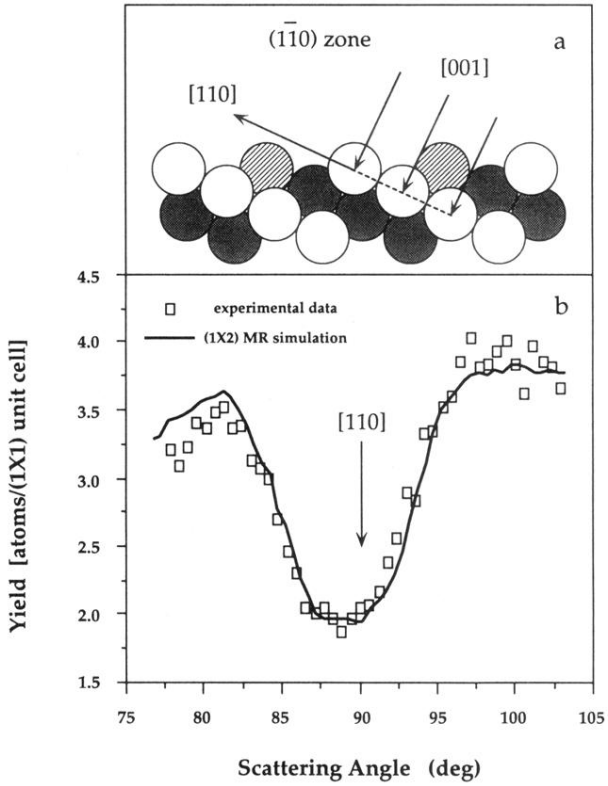

FIG. 7. (a) Scattering geometry for protons incident along the [001] direction and detected in an angular range including the [110] direction in the $(1\bar{1}0)$ plane. The lightly shaded atoms are the missing atoms in the same plane as the heavily shaded atoms. (b) Experimental data (open squares) and the unsmoothed simulation for our optimum structure (solid line) as a function of scattering angle for 100-keV protons. The crystallographic direction associated with the bulk blocking dip is indicated.